

# 635 nm femtosecond fiber laser oscillator and amplifier

Jinhai Zou<sup>a,b,†</sup>, Qiujun Ruan<sup>a,b,†</sup>, Tingting Chen<sup>b</sup>, Hang Wang<sup>a</sup>, Luming Song<sup>a</sup>, Yikun Bu<sup>a</sup>, and Zhengqian Luo<sup>a,b,\*</sup>

<sup>a</sup>Xiamen University, School of Electronic Science and Engineering, Fujian Key Laboratory of Ultrafast Laser Technology and Applications, Xiamen, China

<sup>b</sup>Shenzhen Research Institution of Xiamen University, Shenzhen, China

**Abstract.** Although visible femtosecond lasers based on nonlinear frequency conversion of Ti:sapphire femtosecond oscillators or near-infrared ultrafast lasers have been well developed, limitations in terms of footprint, cost, and efficiency have called for alternative laser solutions. The fiber femtosecond mode-locked oscillator as an ideal solution has achieved great success in the 0.9 to 3.5  $\mu\text{m}$  infrared wavelengths, but remains an outstanding challenge in the visible spectrum (390 to 780 nm). Here, we tackle this challenge by introducing a visible-wavelength mode-locked femtosecond fiber oscillator along with an amplifier. This fiber femtosecond oscillator emits red light at 635 nm, employs a figure-nine cavity configuration, applies a double-clad  $\text{Pr}^{3+}$ -doped fluoride fiber as the visible gain medium, incorporates a visible-wavelength phase-biased nonlinear amplifying loop mirror (PB-NALM) for mode locking, and utilizes a pair of customized high-efficiency and high-groove-density diffraction gratings for dispersion management. Visible self-starting mode locking established by the PB-NALM directly yields red laser pulses with a minimum pulse duration of 196 fs and a repetition rate of 53.957 MHz from the oscillator. Precise control of the grating pair spacing can switch the pulse state from a dissipative soliton or a stretched-pulse soliton to a conventional soliton. In addition, a chirped-pulse amplification system built alongside the oscillator immensely boosts the laser performance, resulting in an average output power over 1 W, a pulse energy of 19.55 nJ, and a dechirped pulse duration of 230 fs. Our result represents a concrete step toward high-power femtosecond fiber lasers covering the visible spectral region and could have important applications in industrial processing, biomedicine, and scientific research.

Keywords: fiber lasers; visible lasers; mode locking; femtosecond laser.

Received Jan. 30, 2024; accepted for publication Feb. 6, 2024; published online Feb. 29, 2024.

© The Authors. Published by SPIE and CLP under a Creative Commons Attribution 4.0 International License. Distribution or reproduction of this work in whole or in part requires full attribution of the original publication, including its DOI.

[DOI: [10.1117/1.APN.3.2.026004](https://doi.org/10.1117/1.APN.3.2.026004)]

## 1 Introduction

The emergence of ultrafast laser pulse generation, a milestone in laser science, has triggered incredible progress across a wide array of disciplines, encompassing industrial applications, energy technologies, life sciences, and beyond.<sup>1,2</sup> Cutting-edge innovations, such as robust laser ignition systems,<sup>3</sup> vibrant laser 3D printing,<sup>4</sup> mind-boggling attosecond science,<sup>5</sup> and high-resolution microscopic imaging,<sup>6</sup> are effectively powered by ultrafast lasers. Among the various laser platforms that have been developed, fiber oscillators, esteemed for their compact design, outstanding performance, and cost-effectiveness, have

become one of the mainstream technologies for generating femtosecond laser pulses.<sup>7-14</sup> However, their operating wavelengths have been predominantly limited to the range between 0.9 and 3.5  $\mu\text{m}$  near-infrared and mid-infrared spectral region,<sup>10,13</sup> which has, in turn, restricted their applicability in numerous applications that require light sources at the visible wavelengths (390 to 780 nm). Over the past decades, the expansion of compact femtosecond fiber oscillators into the previously uncharted visible wavelength range has always been a challenging but passionate pursuit in laser science.

Visible femtosecond lasers stand as pivotal light sources, offering distinct advantages in special material precision processing, high-resolution fluorescence microscopy, optical atomic clocks, and other applications.<sup>15-19</sup> Generation of visible femtosecond lasers was predominantly based on Ti:sapphire

\*Address all correspondence to Zhengqian Luo, [zqluo@xmu.edu.cn](mailto:zqluo@xmu.edu.cn)

<sup>†</sup>These authors contributed equally to this work.

femtosecond oscillators<sup>20</sup> or harnessing the nonlinear frequency conversion (e.g., frequency doubling,<sup>21</sup> sum frequency,<sup>22</sup> and optical parametric process<sup>23</sup>) until recently. Ti:sapphire femtosecond oscillators and parametric amplifiers are renowned for their capability of producing high-performance femtosecond lasers, as well as notorious for high costs, intricate maintenance requirements, and unwieldy dimensions. On the other hand, nonlinear frequency conversion, though widely used to generate visible femtosecond lasers at multiple wavelengths, faces challenges, such as system complexities, high cost, and a compromise in laser performance (e.g., stability and noise) stemming from nonlinear conversion processes. Fiber laser oscillators are often regarded as an attractive solution to overcome these limitations. While direct generation of femtosecond pulses from mode-locked fiber oscillators operating in the infrared range (0.9 to 3.5  $\mu\text{m}$ ) has seen substantial advancements in the past decades, it has not yet been realized in the visible spectrum (390 to 780 nm).

Currently, the majority of visible fiber lasers leverage rare-earth-doped fluoride fibers (e.g.,  $\text{Pr}^{3+}$ ,<sup>24</sup>  $\text{Ho}^{3+}$ ,<sup>25</sup>  $\text{Dy}^{3+}$ ,<sup>26</sup> and  $\text{Er}^{3+}$ <sup>27</sup>) as the efficient gain medium. Over the years, significant progress has been made in achieving wavelength-tunable,<sup>28–30</sup> high-power,<sup>31–37</sup> Q-switched,<sup>38–40</sup> and mode-locked<sup>41–46</sup> visible rare-earth-doped fluoride fiber lasers. Although it has been very well demonstrated in the near-infrared, femtosecond mode locking in visible fiber lasers remains extraordinarily challenging and has not yet been reported, except for one related work on 1.6 ps visible fiber oscillator compressed to 168 fs duration outside the oscillator by a grating pair.<sup>46</sup> This challenge arises from several factors: (1) The underdevelopment of ultrafast optic components designed for the visible-wavelength range; (2) the limited availability of high-performance fast optical modulators or mode lockers at visible wavelengths; and (3) the extreme positive dispersion presented in visible fiber laser cavities, which hinders the initiation of stable femtosecond mode locking. In recent years, mode-locked femtosecond fiber oscillators in the near-infrared regions using a phase-biased nonlinear amplifying loop mirror have gained considerable attention.<sup>47–52</sup> These laser oscillators employ a phase-bias mechanism, often realized through a phase shifter, to get rid of the long intracavity fibers for nonlinear phase shift accumulation. This innovative approach typically not only facilitates higher mode-locking repetition rates, enhanced tuning flexibility, and long-life operation<sup>10,47</sup> but also provides a chance to manage the total cavity dispersion in a larger parameter space from the normal to the abnormal regime. When implementing such a mode-locking mechanism in visible rare-earth-doped fiber lasers, the dominant normal dispersion in the entire cavity mainly originates from the gain fiber, which should be feasible to compensate if a short and high-gain fiber is used. In this case, a low-loss dispersion compensation component at visible wavelength becomes a key element to adjust the net cavity dispersion for successful initiation of solitons.

In this paper, we present an experimental demonstration of a visible-light mode-locked femtosecond fiber oscillator based on a high-gain  $\text{Pr}^{3+}$ -doped fiber and a pair of customized diffraction gratings for dispersion management. The oscillator achieves remarkably stable self-starting mode locking, building upon the phase-biased NALM, yielding laser pulses with a central wavelength of 635.5 nm, a widest 3-dB bandwidth of 5.4 nm, a minimum pulse duration of 196 fs, and a repetition rate of 53.957 MHz. By manipulating the intracavity dispersion

and polarization, we have observed multiple mode-locking states, including conventional solitons, dispersion-managed solitons, dissipative solitons, and bound-state solitons. To further enhance the laser performance to fulfill more general application purposes, we have constructed a visible chirped-pulse amplification (CPA) system and improved the average power  $>1$  W while maintaining a compressed pulse duration of 230 fs. This laser architecture with dispersion management capabilities thus serves as a testbed to explore complex ultrafast soliton dynamics in the visible-wavelength region and paves the way for implementing miniaturized visible fiber femtosecond laser sources with broader spectral range, narrower pulse width, and higher power, enabling a wide range of applications.

## 2 Experimental Setup and Operation Principle

Figure 1 shows a detailed schematic of the visible-wavelength femtosecond fiber oscillator and amplifier system. The fiber used in the oscillator is a 2.3-m double-clad (DC)  $\text{Pr}^{3+}$ -doped fluoride fiber, which is manufactured by Le Verre Fluoré and boasts the following specifications: a  $\text{Pr}^{3+}$  doping concentration of 8000 ppm (wt.), a core diameter of 7.5  $\mu\text{m}$ , a core numerical aperture (NA) of 0.08, an inner-clad profile in a double D-shaped configuration with dimensions of 115  $\mu\text{m}$  by 125  $\mu\text{m}$ , an inner-clad NA of 0.45, an inner-clad absorption coefficient of 2.1 dB/m at 443 nm, a core group velocity dispersion (GVD) coefficient ( $\beta_2$ ) of  $+0.0708$  ps<sup>2</sup>/m at 635 nm, and a core nonlinear coefficient ( $\gamma$ ) of  $0.0049$  W<sup>-1</sup> · m<sup>-1</sup>. The gain fiber is efficiently pumped directly by a 443 nm laser diode (LD) through a collimator, generating a strong red-light gain. The transition diagram is as below: (1)  $^3\text{P}_2$  level is excited by ground state absorption of the  $^3\text{H}_4$  level with the 443 nm LD, (2) non-radiative relaxation ensues from  $^3\text{P}_2$  to  $^3\text{P}_0$ , and (3) radiative transition occurs from  $^3\text{P}_0$  to  $^3\text{F}_2$ , generating strong emission at  $\sim 635$  nm.<sup>34</sup> Other important components of the oscillator include a homemade dichroic mirror (DM), five wavelength plates, a polarization beam splitter (PBS), a homemade 10:90 beam splitter (BS), a Faraday rotator (FR), and a homemade high-reflective coating mirror. The coating mirrors (DM, BS, and mirror) are manufactured by coating on fused quartz substrates with  $\text{SiO}_2/\text{Ta}_2\text{O}_5$  dielectric films using an ion beam-assisted deposition system (DJ-800, Golden Vacuum). We have also customized a pair of visible transmission gratings with high efficiency ( $>93\%$  at 635 nm) and high groove density (1739.1 lines/mm) to minimize the cavity loss and manage total dispersion. The gratings operate near the Littrow configuration, featuring an incident angle of  $\sim 31.4$  deg, and providing a GVD coefficient of  $-5.116$  ps<sup>2</sup>/m at 635 nm. The intracavity net dispersion is calculated to be  $+0.055$  ps<sup>2</sup> with a grating spacing of 21 mm. The red laser obtained from one collimator accumulates an additional  $\pi/2$  phase shift after traversing the phase shifter comprising the FR and eighth-wave plate twice, and then enters the other collimator, thereby facilitating self-starting mode locking at a low threshold.<sup>10</sup> The gratings are introduced strategically to regulate intracavity dispersion for initiating different mode-locking operations (e.g., conventional soliton, dispersion-managed soliton, and dissipative soliton). Furthermore, the oscillator incorporates two half-wave plates and two quarter-wave plates to fine-tune intracavity polarization. It is essential to note that to achieve stable mode-locking operation in the few-mode gain fiber, loops with a radius of  $\sim 2$  cm are placed on

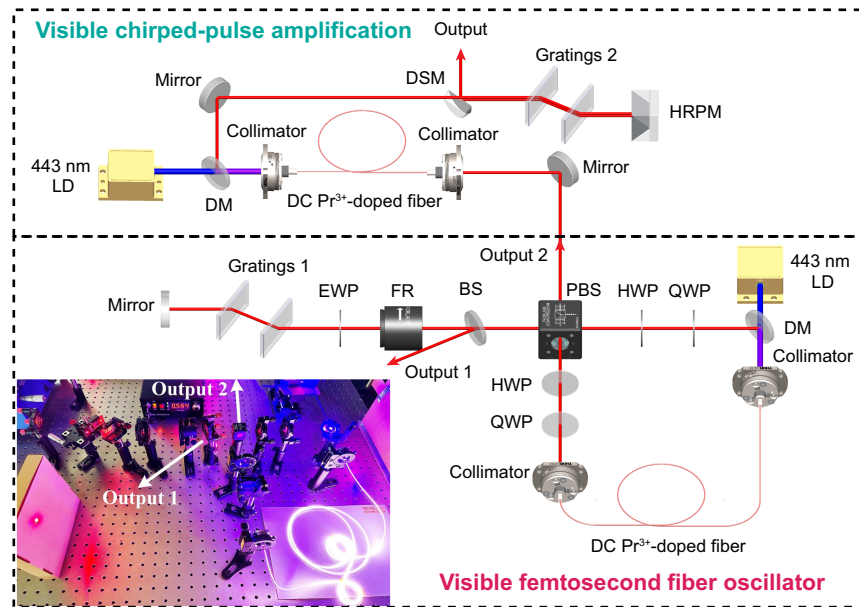


**Fig. 1** Schematic of visible femtosecond fiber oscillator and amplifier. The inset shows the photograph of the visible femtosecond fiber oscillator. DM, dichroic mirror; HWP, half-wave plate; QWP, quarter-wave plate; EWP, eighth-wave plate; PBS, polarization beam splitter; BS, beam splitter; FR, Faraday rotator; Gratings, a pair of transmission gratings; Mirror, high-reflective coating mirror; DSM, D-shaped mirror; HRP, hollow roof prism mirror.

both sides of the fiber to suppress higher-order modes (see the inset of Fig. 1), which bring very little additional loss to the fundamental mode. To further obtain a high-power visible femtosecond laser, the output laser of the oscillator is amplified by the visible CPA system. The system comprises a 2.5 m DC Pr<sup>3+</sup>-doped fluoride fiber, a 433 nm LD, a DM, two collimators, and a grating pair compressor. The compressor includes a D-shaped mirror, a hollow roof prism mirror (HRPM), and a pair of transmission gratings with a groove density of 1398.6 lines/mm. In the experiment, the optical spectrum is captured using a 350 to 1750 nm optical spectrum analyzer with a resolution of 0.05 nm (AQ-6315E, Ando). The pulse train and radio-frequency (RF) spectrum are recorded by a 12.5-GHz photodetector (ET-4000F, Electro-Optics Technology, Inc.) in conjunction with a 12-GHz, 40 GS/s oscilloscope (DSO81204A, Agilent Infiniium), or an electrical spectrum analyzer (N9020A, Agilent). The pulse duration is determined by an autocorrelator (FR-103XL, Femtochrome), and the power measurements are conducted using a 350 to 1100 nm optical power meter (S142C, Thorlabs, Inc.). In addition, a DM is also used to filter out the remaining pump power (443 nm) when measuring the output laser power of the PBS.

### 3 Results and Discussion

#### 3.1 Visible Femtosecond Fiber Oscillator

In the experiment, the threshold of the continuous-wave (CW) laser is  $\sim 1.08$  W. As the pump power is incrementally raised to 1.63 W, a notable transition occurs where self-starting mode-locking pulses can be observed in the oscilloscope. At this stage, the mode-locked pulse exhibits a multipulse operation, and the transition to stable single-pulse mode locking is achieved by reducing the pump power accordingly. Figure 2 shows the

typical output characteristics of the red-light mode-locked femtosecond fiber oscillator under 1.33 W pump power. As shown in Fig. 2(a), the mode-locked optical spectrum manifests a central wavelength of 635.5 nm, accompanied by a 3-dB bandwidth of 4.1 nm. Figure 2(b) gives the typical pulse train with a pulse interval of 18.5 ns, and their pulses have uniform pulse intensity, as evidenced by the inset in Fig. 2(b), underscoring the exceptional stability of the mode-locking operation. Figure 2(c) shows the intensity autocorrelation trace of the output pulses, aptly fitted by a sech<sup>2</sup> function, revealing a pulse duration as short as 199 fs. In addition, as shown in Fig. 2(d), the output RF spectrum has a fundamental frequency of 53.957 MHz and a high signal-to-noise ratio of  $\sim 78.7$  dB. What the inset of Fig. 2(d) shows is particularly noteworthy, as it demonstrates the absence of spectral modulation within the 3 GHz-span RF spectrum, which serves as a compelling testament to the stable mode locking of the oscillator. In addition, the beam quality parameter ( $M_{x,y}^2$ ) of the output laser was measured to be 1.43 and 1.47, indicating the oscillator is almost a single-mode operation.

To better understand the mode-locking behavior of the fiber oscillator, the mode-locked evolution with different pump powers is further investigated. Figure 3(a) shows the progression of the optical spectrum versus the pump power. One can, interestingly, see that when the pump power increases, the spectral bandwidth emerges according to the law of recurrent broadening and decreasing. This intriguing behavior could potentially be attributed to the splitting of time-domain pulses into the bound-state pulses with the increase of the pump power [see Fig. 3(b)]. Figure 3(b) also reveals that the temporal separation of the bound-state pulses is about 18.9 ps, corresponding to the spectral modulation of 0.071 nm. It is worth noting that this spectral modulation remains undetected in the spectra due to the low resolution (0.05 nm) of the optical spectrum analyzer. To gain further insights, we meticulously documented the

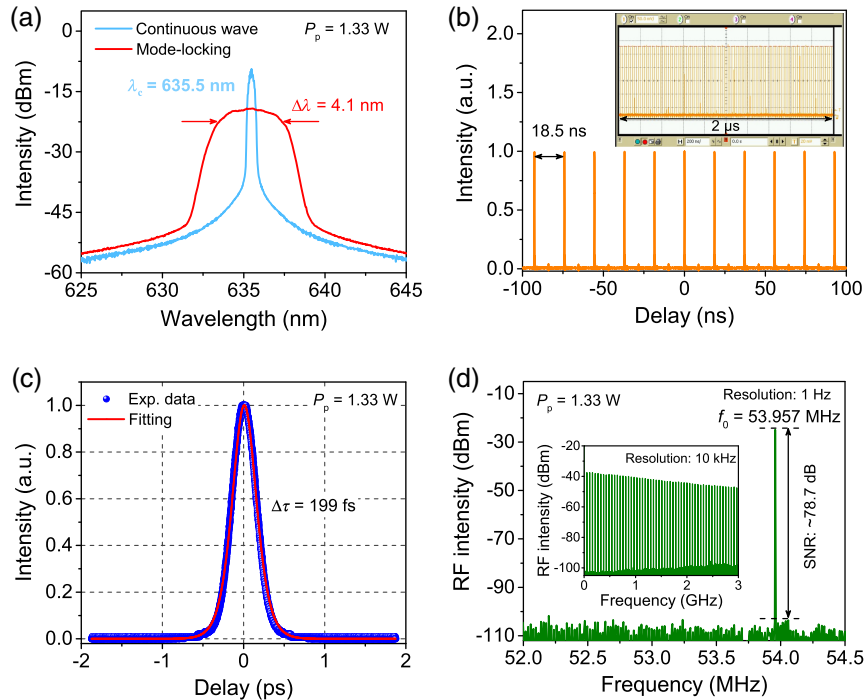


**Fig. 2** Typical characteristics of visible mode-locked femtosecond fiber oscillator under the dispersion of  $+0.055 \text{ ps}^2$ . (a) Optical spectra of mode locking and CW operations. (b) Oscilloscope trace of the pulse train (inset, a screenshot of oscilloscope trace). (c) Autocorrelation trace of the output pulses. (d) RF spectrum at the fundamental frequency [inset, a broadband RF spectrum (3 GHz span)].

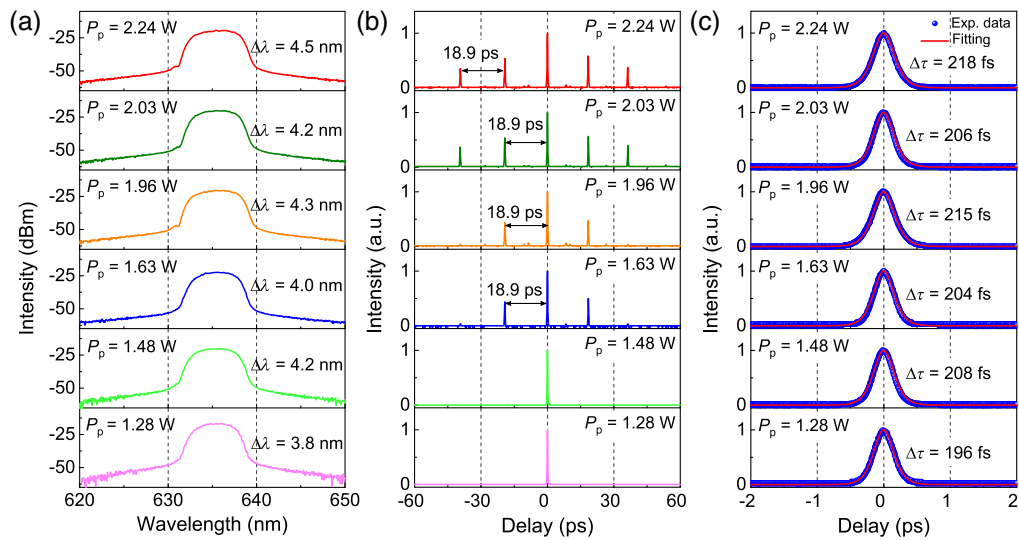


**Fig. 3** Evolution of visible femtosecond fiber oscillator with different pump powers under the dispersion of  $+0.055 \text{ ps}^2$ . (a) Optical spectra output from the BS, (b) the corresponding autocorrelation traces, and (c) a close look of autocorrelation traces (4-ps span).

corresponding narrow-range autocorrelation traces (i.e., single-pulse envelope), as shown in Fig. 3(c). Remarkably, under a 1.28 W pump power, an impressive minimum pulse duration of 196 fs is achieved. Furthermore, the pulse duration of these single pulses shows the same trend as the spectral bandwidth, with the pump power incrementally increasing. The results are

also interesting and critical, as they show the potential to explore complex soliton dynamics with this simple cavity via power and polarization adjustment.

Figure 4(a) offers the average output power of the 635 nm femtosecond laser concerning the pump power. Both the average output power of the BS (output 1) and the PBS (output 2)

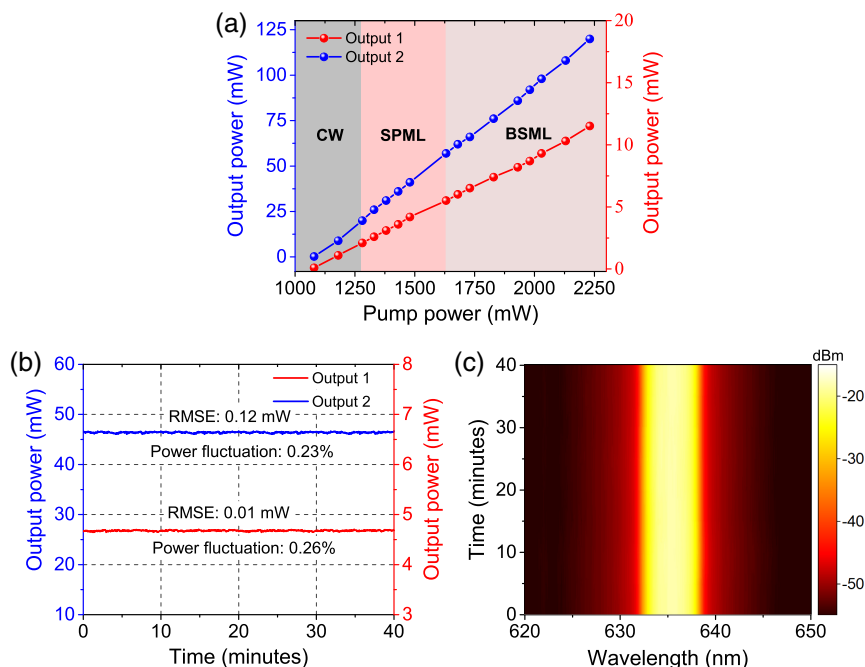


**Fig. 4** Output characterization of 635 nm femtosecond fiber laser oscillator under the dispersion of  $+0.055 \text{ ps}^2$ . (a) Average output powers from the BS (output 1) and PBS (output 2). (b) Power stability curve of the femtosecond laser at the pump power of 1.53 W. (c) Stability measurement of the mode-locked spectrum under 1.53 W pump power.

exhibits a linear increase without any saturation. Impressively, under a pump power of 2.23 W, we achieved maximum output powers of 11.5 and 120 mW for the BS and PBS, respectively. In addition, under a pump power of 1.48 W, the output powers are 4.2 and 41 mW for the BS and PBS, respectively, with calculated single-pulse energies of 0.078 and 0.76 nJ. Figure 4(a) also shows the oscillator works in single-pulse mode locking within the pump power range of 1.28 to 1.63 W, and as the pump power further increases, the operation becomes bound-state mode locking (also see Fig. 3). To assess the operational stability of the mode-locked femtosecond fiber oscillator, as shown in Fig. 4(b), we recorded the output powers and optical spectra over 40 min under a pump power of 1.53 W. Notably, the RMSEs in both BS and PBS output are 0.01 and 0.12 mW, and the corresponding fluctuations are 0.26% and 0.23%, respectively, illustrating the outstanding stability of the oscillator. In addition, as shown in Fig. 4(c), both the central wavelength and spectral bandwidth of the oscillator remained remarkably stable during the entire 40-min test, displaying no discernible drift or changes, which also indicates the excellent long-term stability of the oscillator. Finally, the relative intensity noise (RIN) is also measured by an RF spectrum analyzer (N9020A, Agilent) together with a Si photodetector (PDA36A2, Thorlabs) for  $>10 \text{ Hz}$  Fourier frequency. The observed RIN shows a floor between  $-120$  and  $-90 \text{ dB/Hz}$  for low frequencies, which is attributed to the instability of free-space components and the power and frequency fluctuations of the pump laser.

In addition, the pulse duration of the mode-locked laser is intricately linked to the net dispersion, which can be finely controlled by regulating the spacing of the intracavity gratings. In our experiment, we systematically explored the influence of various net dispersion regimes on the mode-locking performance by tuning the grating pair interval under a pump power

of 1.33 W. The outcomes are presented in Fig. 5 (also see Video 1). Figures 5(a) and 5(b) show a comprehensive view of the optical spectra and the corresponding autocorrelation traces from the output of BS (output 1). When the net dispersion is adjusted to  $+0.002 \text{ ps}^2$ , a broadest spectral 3-dB bandwidth of 5.4 nm along with a pulse duration of 900 fs can be achieved. The spectral bandwidth of 5.4 nm supports the Fourier transform limit duration of  $\sim 79 \text{ fs}$  for a sech<sup>2</sup> pulse. Notably, when the net dispersion is set to  $+0.055 \text{ ps}^2$ , we attain the narrowest pulse duration of 199 fs, accompanied by a spectral bandwidth of 4.1 nm, and the time-bandwidth product (TBP) is calculated as 0.61, close to the Fourier-transform limit of a sech<sup>2</sup> pulse. Turning our attention to the output of the PBS (output 2), as shown in Figs. 5(c) and 5(d), we observe a similar trend in spectral bandwidth with varying net dispersion. Specifically, the obtained widest spectral bandwidth is also at  $+0.002 \text{ ps}^2$ , which is like the output of the BS. Intriguingly, the minimum pulse duration is realized at a net dispersion of  $-0.057 \text{ ps}^2$ , corresponding to a pulse duration of 460 fs, and the TBP is calculated as 0.62. It can also be seen from Fig. 5(d) that with the net dispersion from  $+0.087$  to  $-0.0241 \text{ ps}^2$ , the TBP of the mode-locked laser output from the PBS shows a decreasing trend. Besides, it is noteworthy that adjusting the net dispersion to either large net-anomalous or net-normal values results in a narrowing of the spectral bandwidth, as is evident in Figs. 5(a) and 5(c). Specifically, when the net dispersion is set to  $-0.0241 \text{ ps}^2$  (pink curve) and  $+0.087 \text{ ps}^2$  (red curve), the mode-locked spectra exhibit the typical peculiarities of traditional soliton and dissipative soliton, respectively. These findings underscore the versatility of the oscillator in tailoring its output characteristics through precise control of net dispersion, offering opportunities for customizing laser performance for specific applications.

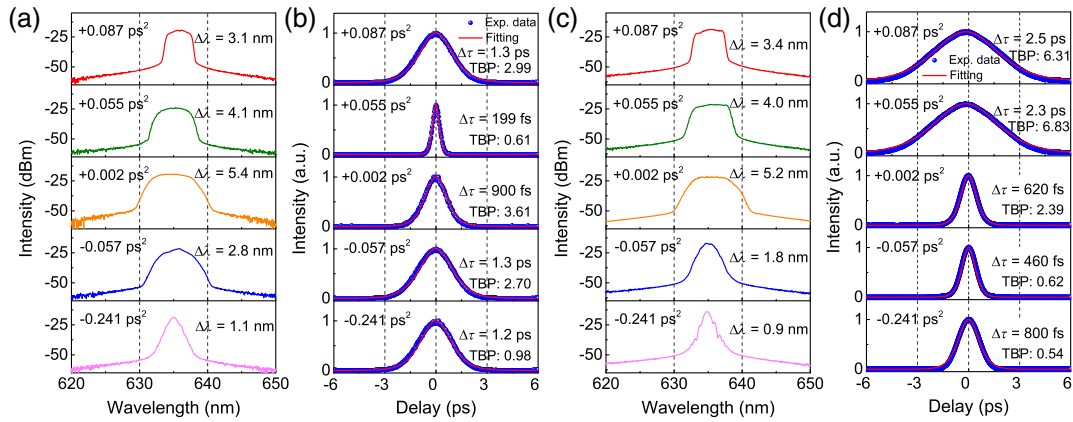


**Fig. 5** Characteristics of visible fiber oscillator under different net dispersions at 1.33 W pump power. (a) Optical spectra output from the BS (output 1), and (b) the corresponding autocorrelation traces. (c) Optical spectra output from the PBS (output 2), and (d) the corresponding autocorrelation traces (Video 1, MP4, 3.96 MB [URL: <https://doi.org/10.1117/1.APN.3.2.026004.s1>]).

### 3.2 Visible Chirped-Pulse Amplification

Subsequently, in the pursuit of high-power visible femtosecond laser output, a visible CPA system was used to amplify the output laser pulses generated by the oscillator. To optimize the amplification process and mitigate nonlinear effects and amplified spontaneous radiation, we strategically selected the laser pulses originating from the PBS output, characterized by a net dispersion of  $+0.087 \text{ ps}^2$ , as the seed laser. This choice was driven not only by its highest output power but also by its relatively wide spectral bandwidth (meaning the potential for duration compression), also considering that dissipative soliton is suitable to achieve larger pulse energy. In the experiment, the laser pulses emanating from the oscillator undergo stretching

from 2.6 to 8.6 ps when traversing the 2.5 m DC  $\text{Pr}^{3+}$ -doped fluoride fiber and then are subjected to amplification by the red-light fiber amplifier. Subsequently, the amplified laser pulses are compressed through the grating pair compressor. The results of this amplification and compression are shown in Fig. 6. Figure 6(a) gives the amplified spectra under different pump powers. Notably, the spectral bandwidth narrows as the pump power increases, which is attributed to gain narrowing within the amplifier. Impressively, this amplification process yields a maximum average power of 1055 mW, and the corresponding pulse energy is counted as 19.55 nJ, as shown in Fig. 6(b). Furthermore, the grating pair compressor effectively dechirps the pulse duration to 230 fs, as showcased in Fig. 6(c). There is no doubt that higher power is available through more

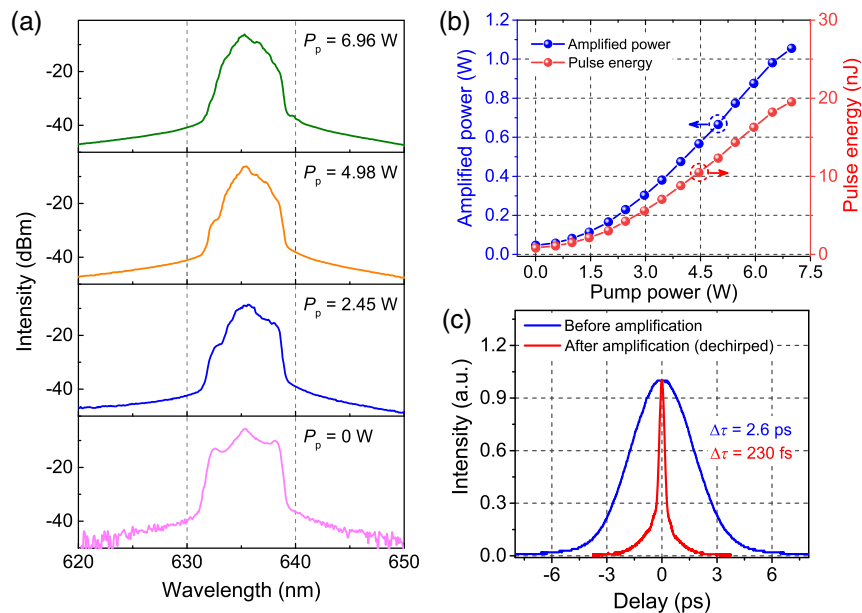


**Fig. 6** Characteristics of visible fiber CPA. (a) Optical spectra under different pump powers. (b) Amplified average power and pulse energy versus the pump power. (c) Autocorrelation traces before and after amplification.

stages of amplification. These results also underscore the efficacy of the visible CPA system in significantly boosting the power of the visible femtosecond laser while maintaining excellent pulse quality, making it a valuable tool for various applications, such as materials processing, biomedical research, and nonlinear optics.

## 4 Conclusion

In summary, we successfully demonstrated a 635 nm soliton mode-locked femtosecond fiber oscillator built upon the phase-biased NALM. This oscillator achieves remarkably stable self-starting mode locking, which delivers laser pulses with a central wavelength of 635.5 nm, a broadest 3-dB bandwidth of 5.4 nm, a minimum pulse duration of 196 fs, and a repetition rate of 53.957 MHz. With the precise tuning of the intracavity gratings, we can easily manipulate the cavity in anomalous, near-zero, and normal dispersion regimes. The dispersion management in this manner not only offers the opportunity to study the fruitful soliton dynamics in the visible range but also allows versatile control over laser parameters, such as pulse duration and spectral bandwidth. By implementing a chirped-pulse fiber amplification system, we further promote the laser output from the oscillator to an unprecedented power exceeding 1 W in the visible fiber lasers while maintaining excellent pulse quality. The achieved laser source could already find enormous applications ranging from advanced materials processing to biomedical and nonlinear optics. Due to the exceptional heat dissipation of fibers, the whole laser system operates with excellent long-time stability, characterized by a low power deviation of <0.3% and negligible wavelength drift. Our soliton mode-locked fiber oscillator and amplifier system bridges the gap in sourcing femtosecond laser pulses from visible fiber lasers, marking a substantial breakthrough in the realm of ultrafast laser technology. This architecture, featuring by compact design, high-performance output, reliable operation, and flexible tunability, can be readily implemented to broaden the mode-locking spectral range, covering the entire visible spectrum. We anticipate immediate applications and stimulation to further activities of such femtosecond fiber laser systems in scientific research, medicine, and biological imaging.

## Code and Data Availability

All the data that support the findings of this study are available from the corresponding author upon reasonable request.

## Acknowledgments

This work was supported by the National Natural Science Foundation of China (Grant Nos. 62022069, 62235014, and 62305275), the Shenzhen Science and Technology Projects (Grant No. JCYJ20210324115813037), and the China National Postdoctoral Program for Innovative Talents (Grant No. BX20230199). The authors declare no conflicts of interest.

## References

1. M. E. Fermann and I. Hartl, "Ultrafast fibre lasers," *Nat. Photonics* **7**(11), 868–874 (2013).
2. M. Malinauskas et al., "Ultrafast laser processing of materials: from science to industry," *Light Sci. Appl.* **5**(8), e16133 (2016).
3. D. Graham-Rowe and R. Won, "Lasers for engine ignition," *Nat. Photonics* **2**(9), 515–517 (2008).
4. K. Sugioka and Y. Cheng, "Ultrafast lasers-reliable tools for advanced materials processing," *Light Sci. Appl.* **3**(4), e149 (2014).
5. P. Á. Corkum and F. Krausz, "Attosecond science," *Nat. Phys.* **3**(6), 381–387 (2007).
6. H. He et al., "Deep-tissue two-photon microscopy with a frequency-doubled all-fiber mode-locked laser at 937 nm," *Adv. Photonics Nexus* **1**(2), 026001 (2022).
7. F. Wang et al., "Wideband-tuneable, nanotube mode-locked, fibre laser," *Nat. Nanotechnol.* **3**(12), 738–742 (2008).
8. Z. Sun et al., "Graphene mode-locked ultrafast laser," *ACS Nano* **4**(2), 803–810 (2010).
9. A. Martinez and Z. Sun, "Nanotube and graphene saturable absorbers for fibre lasers," *Nat. Photonics* **7**(11), 842–845 (2013).
10. M. Li et al., "Mode-locked femtosecond 910 nm Nd: fibre laser with phase biased non-linear loop mirror," *Electron. Lett.* **53**(22), 1479–1481 (2017).
11. R. I. Woodward et al., "Generation of 70-fs pulses at 2.86  $\mu\text{m}$  from a mid-infrared fiber laser," *Opt. Lett.* **42**(23), 4893–4896 (2017).
12. R. Woodward, M. Majewski, and S. Jackson, "Mode-locked dysprosium fiber laser: picosecond pulse generation from 2.97 to 3.30  $\mu\text{m}$ ," *APL Photonics* **3**(11), 116106 (2018).
13. J. Ma et al., "Review of mid-infrared mode-locked laser sources in the 2.0  $\mu\text{m}$ -3.5  $\mu\text{m}$  spectral region," *Appl. Phys. Rev.* **6**(2), 021317 (2019).
14. Y. Han et al., "Generation, optimization, and application of ultrashort femtosecond pulse in mode-locked fiber lasers," *Progr. Quantum Electron.* **71**, 100264 (2020).
15. K. Furusawa et al., "Ablation characteristics of Au, Ag, and Cu metals using a femtosecond Ti:sapphire laser," *Appl. Phys. A* **69**, S359–S366 (1999).
16. J. Krüger and W. Kautek, "Femtosecond pulse visible laser processing of fibre composite materials," *Appl. Surf. Sci.* **106**, 383–389 (1996).
17. Z. Lin and M. Hong, "Femtosecond laser precision engineering: from micron, submicron, to nanoscale," *Ultrafast Sci.* **2021**, 9783514 (2021).
18. G. Hüttmann, C. Yao, and E. Endl, "New concepts in laser medicine: towards a laser surgery with cellular precision," *Med. Laser Appl.* **20**(2), 135–139 (2005).
19. A. D. Ludlow et al., "Optical atomic clocks," *Rev. Mod. Phys.* **87**(2), 637–701 (2015).
20. A. Bartels, D. Heinecke, and S. A. Diddams, "Passively mode-locked 10 GHz femtosecond Ti:sapphire laser," *Opt. Lett.* **33**(16), 1905–1907 (2008).
21. M. K. Shukla, S. Kumar, and R. Das, "Single-pass, efficient type-I phase-matched frequency doubling of high-power ultrashort-pulse Yb-fiber laser using  $\text{LiB}_3\text{O}_5$ ," *Appl. Phys. B* **122**, 1–6 (2016).
22. K. Moutzouris et al., "Sum frequency generation of continuously tunable blue pulses from a two-branch femtosecond fiber source," *Opt. Commun.* **274**(2), 417–421 (2007).
23. J. Cao et al., "Femtosecond OPO based on MgO: PPLN synchronously pumped by a 532 nm fiber laser," *Laser Phys.* **27**(5), 055402 (2017).
24. R. Smart et al., "CW room temperature operation of praseodymium-doped fluorozirconate glass fibre lasers in the blue-green, green and red spectral regions," *Opt. Commun.* **86**(3–4), 333–340 (1991).
25. S. Ji et al., "High power downconversion deep-red emission from  $\text{Ho}^{3+}$ -doped fiber lasers," *Nanophotonics* **11**(8), 1603–1609 (2022).
26. Y. Fujimoto, O. Ishii, and M. Yamazaki, "Yellow laser oscillation in  $\text{Dy}^{3+}$ -doped waterproof fluoro-aluminate glass fibre pumped by 398.8 nm GaN laser diodes," *Electron. Lett.* **46**(8), 586–587 (2010).
27. Z. Luo et al., "Compact self-Q-switched green upconversion Er: ZBLAN all-fiber laser operating at 543.4 nm," *Opt. Lett.* **41**(10), 2258–2261 (2016).

28. H. Okamoto et al., “Visible–NIR tunable Pr<sup>3+</sup>-doped fiber laser pumped by a GaN laser diode,” *Opt. Express* **17**(22), 20227–20232 (2009).
29. H. Wang et al., “High-efficiency, yellow-light Dy<sup>3+</sup>-doped fiber laser with wavelength tuning from 568.7 to 581.9 nm,” *Opt. Lett.* **44**(17), 4423–4426 (2019).
30. J. Zou et al., “Tunable, continuous-wave, deep-ultraviolet laser generation by intracavity frequency doubling of visible fiber lasers,” *J. Lightwave Technol.* **40**(12), 3900–3906 (2022).
31. J. Zou et al., “Direct generation of watt-level yellow Dy<sup>3+</sup>-doped fiber laser,” *Photonics Res.* **9**(4), 446–451 (2021).
32. J. Zou et al., “3.6 W compact all-fiber Pr<sup>3+</sup>-doped green laser at 521 nm,” *Adv. Photonics* **4**(5), 056001 (2022).
33. C. Zhang et al., “Direct generation of 5 W all-fiber red laser at 635 nm,” *Opt. Laser Technol.* **160**, 109050 (2023).
34. E. Kifle et al., “Watt-level visible laser in double-clad Pr<sup>3+</sup>-doped fluoride fiber pumped by a GaN diode,” *Opt. Lett.* **46**(1), 74–77 (2021).
35. M.-P. Lord et al., “2.3 W monolithic fiber laser operating in the visible,” *Opt. Lett.* **46**(10), 2392–2395 (2021).
36. E. Kifle et al., “Deep-red double-clad fiber laser at 717 nm,” *Opt. Lett.* **48**(6), 1494–1497 (2023).
37. J. Zou et al., “4.1 W all-fiber Pr<sup>3+</sup>-doped deep-red laser at 717 nm,” *J. Lightwave Technol.* **42**(1), 332–338 (2024).
38. W. Li et al., “716 nm deep-red passively Q-switched Pr: ZBLAN all-fiber laser using a carbon-nanotube saturable absorber,” *Opt. Lett.* **42**(4), 671–674 (2017).
39. J. Zou et al., “Visible-wavelength all-fiber vortex laser,” *IEEE Photonics Technol. Lett.* **31**(18), 1487–1490 (2019).
40. J. Zou et al., “Visible-wavelength pulsed lasers with low-dimensional saturable absorbers,” *Nanophotonics* **9**(8), 2273–2294 (2020).
41. J. Zou et al., “Towards visible-wavelength passively mode-locked lasers in all-fiber format,” *Light Sci. Appl.* **9**(1), 61 (2020).
42. H. Sun et al., “Visible-wavelength all-fiber mode-locked vortex laser,” *J. Lightwave Technol.* **40**(1), 191–195 (2022).
43. Q. Ruan et al., “Visible-wavelength spatiotemporal mode-locked fiber laser delivering 9 ps, 4 nJ pulses at 635 nm,” *Laser Photonics Rev.* **16**(7), 2100678 (2022).
44. S. Luo et al., “High-power yellow DSR pulses generated from a mode-locked Dy:ZBLAN fiber laser,” *Opt. Lett.* **47**(5), 1157–1160 (2022).
45. S. Luo et al., “Ultrafast true-green Ho:ZBLAN fiber laser inspired by the TD<sub>3</sub> AI algorithm,” *Opt. Lett.* **47**(22), 5881–5884 (2022).
46. M.-P. Lord et al., “Visible femtosecond fiber laser,” *Opt. Lett.* **48**(14), 3709–3712 (2023).
47. G. Liu et al., “Robust 700 MHz mode-locked Yb: fiber laser with a biased nonlinear amplifying loop mirror,” *Opt. Express* **26**(20), 26003–26008 (2018).
48. K. Yin et al., “Self-starting all-fiber PM Er: laser mode locked by a biased nonlinear amplifying loop mirror,” *Chin. Phys. B* **28**(12), 124203 (2019).
49. Y. Song et al., “Tunable all-normal-dispersion femtosecond Yb: fiber laser with biased nonlinear amplifying loop mirror,” *Appl. Phys. Express* **14**(10), 102002 (2021).
50. S. Wang et al., “Femtosecond all-polarization-maintaining Nd fiber laser at 920 nm mode locked by a biased NALM,” *Opt. Express* **29**(23), 38199–38205 (2021).
51. Z.-W. Lin et al., “1.7 μm figure-9 Tm-doped ultrafast fiber laser,” *Opt. Express* **30**(18), 32347–32354 (2022).
52. X. Li et al., “Generation of 978 nm dispersion-managed solitons from a polarization-maintaining Yb-doped figure-of-9 fiber laser,” *Opt. Lett.* **48**(11), 3051–3054 (2023).

**Jinhai Zou** received his BS degree in optoelectronic information science and engineering from China Jiliang University in 2017 and his PhD in electronic science and technology from Xiamen University in 2022. His research focuses on fiber lasers in the visible waveband.

**Qiujun Ruan** received his BS degree in optoelectronic engineering from Huaqiao University in 2014 and his PhD in electronic science and technology from Xiamen University in 2023.

**Zhengqian Luo** received his BS degree in applied physics from Harbin Institute of Technology in 2004 and his PhD in electrical engineering from Xiamen University in 2009. From 2007 to 2009, he studied at Nanyang Technological University as a joint PhD student. He joined Xiamen University as a faculty member in 2010. From 2016 to 2017, he was a visiting professor at the Massachusetts Institute of Technology. Since 2017, he has been a full professor at Xiamen University and currently serves as the head of the Electronic Engineering Department of Xiamen University. His research focuses on ultrafast fiber lasers and on-chip photonic devices. He has published more than 150 journal or conference papers with a total citation of >5500. He is a recipient of the National Science Fund for Excellent Young Scholars and the Fujian Youth Science and Technology Award. He is a senior member of IEEE and served as a young editorial board member for Chinese Laser Press.

Biographies of the other authors are not available.